arXiv:0905.3498v2 [quant-ph] 21 May 2009

Bright and Dark Helices of Light

Ole Steuernagel*
School of Physics, Astronomy and Mathematics, University of Hertfordshire, Hatfield, AL10 9AB, UK
(Dated: May 21, 2009)

Laser beams can be made to form bright and dark intensity helices of light. Such helices have a pitch length on the order of a wavelength and may have important applications in lithography and the manipulation of particles through optical forces. Whereas the form of bright helices is strongly constrained by optical resolution limits the formation of dark helices allows for considerable freedom. It is shown how to arrange dark helices on a grid in massively parallel fashion.

PACS numbers: 42.25.-p, 42.25.Hz, 42.60.Jf, 42.82.Cr, 42.50.Vk

In recent years there has been considerable interest in light beams carrying orbital angular momentum, such as Laguerre-Gauss beams [1]. These are known to have helical wave fronts [1, 2, 3] which have been investigated using interferometric techniques [4, 5, 6]. Yet, little consideration has been given to helical intensity setups, notable exceptions studying bright helices are [7, 8, 9].

Here bright and dark intensity helices of light are introduced in terms of screw dislocations [10] of ordinary standing waves. This allows us to quantify some of their basic characteristics. It is shown that using superpositions with unequal weight to generate the intensity helices allows us to control their widths. Bright helices can only be synthesized with small pitch angles, but there is no upper bound on the pitch gradients of dark helices. Both types can be arranged in large arrays in massively parallel fashion making them potentially suitable for the creation of helical metamaterial using bulk lithography.

Bright and dark interference fringes extending across a standing wave's cross-section are ubiquitous. In optics they have found applications in Lippmann's photography and Gabor's holography, they arise in laser cavities and interferometry and are used as transporters [11] and imaging elements [12] in atom optics. They are on the order of half a wavelength λ of the interfering light apart and since light beams are more than a wavelength wide and can overlap over considerable areas these bright fringes often resemble very tall stacks of pancakes [11]. They can also be slightly modified (the pancakes become deformed), due to the dispersive effects of Gouy's phase, in interfering multimode beams [13]. Instead of using the superposition of identical beams we want to consider the interference between two monochromatic, collinear, counterpropagating partial waves with *different* orbital angular momenta [1, 2]. In this case one can imagine the pancakes (which are centered on the beam axis) to be cut open on one side, then splayed open and glued to the opposing cut faces of their neighbours. In the most tightly wound case such a screw dislocation [10] yields a helix with pitch length $z_1 = \lambda/2$, see Fig. 1. The common pancake stack scenario can be viewed as the special

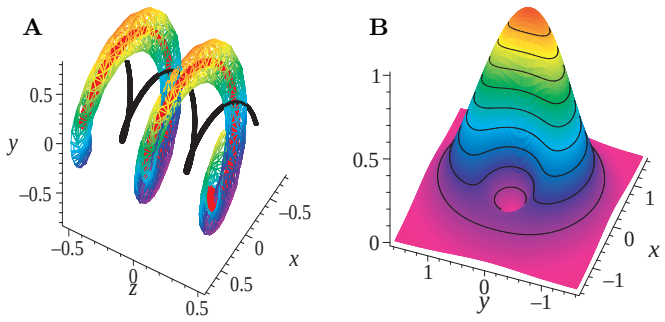

FIG. 1: (Color online) Superposition $\frac{1}{2}u_{0,0}(x,y,z) + u_{0,1}(x,y,-z)$ yields a single bright helix (red line) enveloping a single dark helix (black line) with the minimal pitch $\lambda/2$ [colored mesh was numerically determined as the locations with 90% of peak intensity] (**A**); its focal intensity distribution (**B**). [x- and y-axes in units of focal beam radius w_0, z-axis in units of λ, peak intensity normalized to unity].

case of a degenerate helix with orbital angular momentum difference $l - l' = 0$ and associated pitch length $z_0 = 0$. Alternatively to linking up nearest neighbours, the cut-open pancakes can be connected to their second nearest neighbour with pitch length $z_2 = \lambda$ leaving the nearest neighbour to form part of a second helix on the opposite side of the beam axis, see Fig. 2.

In general the helices' pitch lengths $z_{l-l'}$ (orbital angular momentum quantization implies that l is an integer [1]) are determined by the difference $l - l'$ in orbital angular momentum of the used laser beams and obey $z_{l-l'} = \lambda(l - l')/2$. A negative helix length $z_{l-l'}$ describes inverted handedness. Different superpositions can yield a larger number of intertwined helices and concentric shells of helices, compare Fig. 2. Per nodal shell, there tend to be a number of $|l - l'|$ separate bright helices with dark helically wound regions between them, see references [2, 3] and text following eq. (1) below. Details depend on the mode structures and relative weights of the employed superpositions.

The helices' widths can be controlled through the width of the laser beams' waists $2w_0$. Their lengths are practically limited by the laser beams' divergence. If the beams' cross-sections are elliptically deformed, so are the

*Electronic address: O.Steuernagel@herts.ac.uk

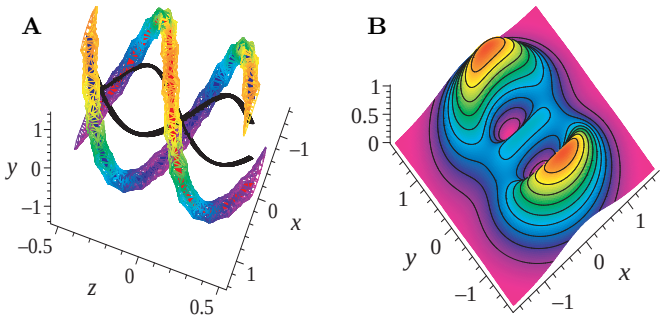

FIG. 2: (Color online) Superposition $u_{0,2}(x,y,z) + \frac{1}{2}u_{1,0}(x,y,-z)$ yields a pair of dark and bright helices with pitch λ (**A**); its focal intensity distribution (**B**) [all units as in Fig. 1, note that compared to Fig. 1 the helices' orientation is reversed].

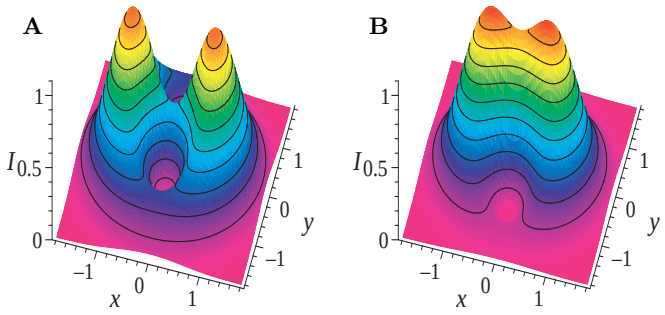

FIG. 3: (Color online) The focal intensity distribution of superpositions $u_{0,2}(x,y,z) + \frac{1}{2}u_{0,0}(x,y,-z)$ (**A**) and $u_{0,2}(x,y,z) + u_{0,0}(x,y,-z)$ (**B**) demonstrate that narrow bright helices self-overlap and become ill defined [all units as in Fig. 1].

helices. Suitable laser beam modes that carry orbital angular momentum, such as Laguerre-Gauss–modes [1], are readily available [2, 3, 4, 5, 14] and the required superpositions are straightforward to implement [15]. The relative phases of the interfering beams can be shifted, this way the intensity-helices revolve around their main axis (including very rapid rotations through frequency detuning between the two opposing beams [14, 16]).

For specificity we will consider the paraxial Laguerre-Gauss modes $U_{p,l}(x,y,z)$ [1, 17] (formed from 'generalized Laguerre polynomials' $L_{p,|l|}$ rather than, say, orbital angular momentum carrying Bessel-beams [9])

$$U_{p,l}\,(z_R,\lambda;r,\phi,z) = \sqrt{\frac{2}{(1+\delta_{0,l})\pi}\frac{p!}{(p+|l|)!}} \times \left(\frac{\sqrt{2}r}{w\,(z)}\right)^{|l|} L_{p,|l|}\left(2\,\frac{r^2}{w\,(z)^2}\right)\left(\frac{e^{il\phi}}{w\,(z)}\right) \times e^{-\frac{r^2}{w(z)^2}} e^{-i(2\,p+|l|+1)\zeta(z)} e^{\frac{ik\,r^2}{2\varrho(z)}}\,\boldsymbol{P}\,. \quad (1)$$

Here λ is the laser's wavelength, $k = 2\pi/\lambda$ its wavenumber and ω the angular frequency of the light; x and y are the transverse coordinates, and z parameterizes the beam axis. Kronecker's δ-function takes care of the correct normalization, the polarization vector $\boldsymbol{P}$ is normalized but does not have to be specified. The azimuthal angle ϕ is connected to the transverse coordinates via the relation $e^{il\phi} = (x+iy)^l$: l is the integer orbital angular momentum index with the associated orbital angular momentum $L_l = \hbar l$ [1, 2]. The discrete radial index p counts the number of nodal rings in the radial direction $r = \sqrt{x^2+y^2}$. The beam radii are given by $w(z) = w_0\sqrt{1+z^2/z_R^2}$ with the beam waist radius $w_0 = \sqrt{\lambda z_R/\pi}$ where z_R is the Rayleigh-length; it also parameterizes the longitudinal Gouy-phase shifts $\zeta(z) = \arctan(z/z_R)$ and the wavefront radii $\varrho(z) = (z^2+z_R^2)/z$ [1, 17].

In order to form bright (or dark) light helices we have to create constructive (or destructive) interference along the entire phase front. For this it suffices to interfere two radially matching pure Laguerre-Gauss laser modes with suitably chosen amplitudes c and c' travelling in opposite directions, namely, to form a superposition

$$\begin{aligned}\boldsymbol{E}\,(x,y,z;t) &= E(x,y,z;t)\,\boldsymbol{P} \\ &= \left[c\,u_{p,l}(x,y,z) + c'u'_{p',l'}(x,y,-z)\right]\cdot e^{-i\omega t}\boldsymbol{P}\,, \end{aligned} \quad (2)$$

where the full paraxial solutions $u_{p,l}(x,y,z) = U_{p,l}(x,y,z)e^{ikz}$ were used. We assume that the laser is uniformly polarized and therefore represent the electric field as a scalar field multiplied with the polarization vector $\boldsymbol{P}$. From this superposition we can extract the spatially fast-oscillating term $e^{i(kz+l\phi)}$ which yields the interference term $\cos(2kz+(l-l')\phi)$. When a full turn ($\Delta\phi = 2\pi$) along the intensity helix is tracked the ensuing shift in the z-direction is

$$z_{l-l'} = (l-l')2\pi/(2k) = \lambda(l-l')/2\,. \quad (3)$$

This confirms the intuitive description in terms of a screw dislocation given above. Note that the interference between two beams travelling in the same direction yields interference fringes [4] but cannot yield helical intensity spirals on the wavelength scale as was suggested in reference [18]; instead it forms intensity rods which are modulated by Gouy's phase thus forming rods with a twist [19] very similar to those displayed in Fig. 1 of reference [20]. Intuitively this should not be too surprising since in a forward-only configuration light following a helical path would travel superluminally. The effects discussed here are not a consequence of Gouy's phase, unlike the helical intensity distributions considered in references [19] and [21] or the nodal lines investigated in reference [15], all giving rise to 'half-oscillations' [13] on the scale of the beam's Rayleigh length.

The effects discussed here necessarily require interference of two counterpropagating partial waves: this implies that the medium needs to be sufficiently transparent. Also note, reflection by a mirror inverts the helicity of a mode and therefore beams carrying orbital angular

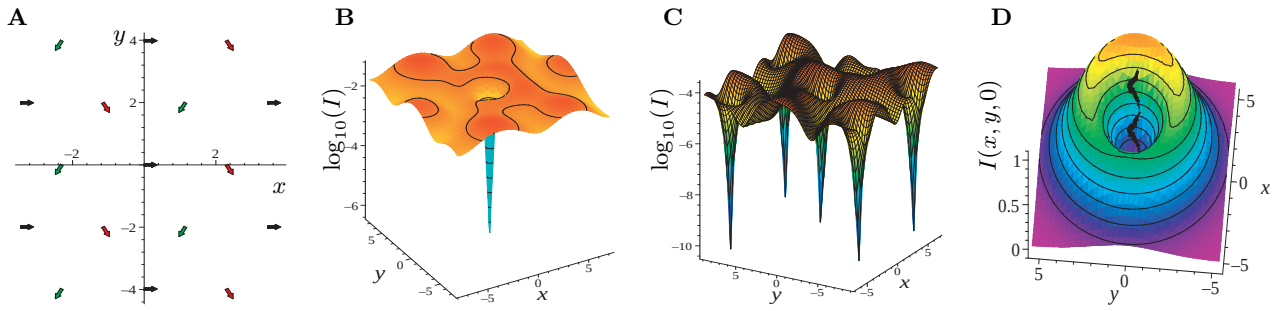

FIG. 4: (Color online) A hexagonal grid of parallel equal Gaussian beams (nearest neighbour distance $2.3\,w_0$) arranged according to three sublattices with different polarization orientations (beam centers and their polarizations indicated by arrows in panel **A**) yields a uniform bright background as is confirmed by the logarithmic intensity plot in the middle panels **B** and **C**. The focal intensity distribution of a dark helices created from the superposition $\frac{1}{8}u_{0,0}(x,y,z) + u_{0,1}(x,y,-z)$ is displayed in panel **D** together with the location of its dark helix as a black line. Such a helix can either be embedded into a uniform background, see countour plot **B**, or many of them can be arranged in a hexagonal grid, see mesh plot **C**. Compared to the plot in panel **B** in panel **C** a slightly wider center-to-center distance of $2.5\,w_0$ was used. This increases both: background fluctuations and pattern contrast. In both cases (**B** and **C**) the dark helices' intensities are at least four orders of magnitude weaker than the background: massively parallel or sparse implementations of dark helices with good contrast are possible.

momentum, within a laser cavity say, form intensity helices (but not single ones since $l - l' \neq 1$ in the reflection case).

Unlike bright features (see Fig. 3), dark features can provide superresolution [22] and therefore allow us to create structures with spatial extensions below the diffraction limit and hence dark helices with large pitch angles. For example, the superposition of an ordinary Gaussian beam $u_{0,0}$ with a Laguerre-Gauss mode with one unit of orbital angular momentum, $E(x,y,z) \propto c \cdot u_{0,0}(x,y,z) + u_{0,1}(x,y,-z)$, forms a single bright and dark helix. In this case the dark helix' radius can be determined analytically from the position of the field's zero at $(x_0, y_0, 0) = (-c\,w_0/\sqrt{2}, 0, 0)$. The stronger the field of the added Gaussian beam the more the zero of the Laguerre-Gaussian mode gets displaced from the beam axis. For small values of c the dark helix is slim and steep since in the focal plane the pitch angle is $\alpha = \arctan((2\pi b\lambda)/(c(-3\lambda + c^2\lambda + 4b\pi))) \approx \arctan(\lambda/(2^{3/2}\pi c w_0))$. This expression of the pitch angle arises from expressions for the focal plane field gradients at the core of the dark helix, specifically: $\partial_x E = 2\sqrt{\pi}\exp(-c^2/2)/(b\lambda)$, $\partial_y E = -i\partial_x E$, and $\partial_z E = 2(-3\lambda + c^2\lambda + 4b\pi)/(2\pi b\lambda) \cdot \partial_y E$. This, in turn, allows us to work out the trapping potentials if the helix is to be used as a blue-detuned, dark helical atom waveguide, similar to the bright case [8]. The dipole-force trapping potential [23] is proportional to $V(x,\eta) \propto (\partial_x E)^2 x^2 + 4(\partial_x E)^2/(1 + [(\partial_y E)/(\partial_z E)]^2)\eta^2)$, where η is the coordinate perpendicular to the local radius vector and the local tangent vector of the dark helix. A closed analytical expression for the position of the helices can be derived for this special case but the expressions are not transparent enough to be of great value, instead an excellent approximation for the positions (x_0, y_0) of dark and bright helices generated by superpositions of the form (2) is given by $(x_0(z) + iy_0(z)) = (x_0(0) + iy_0(0))\sqrt{(1 + z^2/z_R^2)}\exp(i\chi(z))$ with the phase $\chi(z) = -(2(1 + p + p') + |l| + |l'|)\zeta + (l - l')\phi + 2kz$.

It is possible to embed such helical beams into a background of roughly uniform illumination. This is illustrated for a superposition of three triangular lattices with three different polarization directions (Fig. 4 **A**). This hexagonal lattice is tightly packed, yet shows little destructive interference through the suitable choice of the beams' polarizations.

In our examples, this lattice is either filled with ordinary Gaussian $u_{0,0}$-beams (Fig. 4 **B**) or with spiraling beams formed from superpositions (Fig. 4 **C**) such as the one displayed in Fig. 4 **D**. Logarithmic intensity plots show that the background intensity is quite uniform (varies less than an order of magnitude) in both cases, **B** and **C**.

In case **B**, after removal of the central lattice beam at the origin (and additional suppression of the remaining quadratic intensity terms at the origin due to spill-over from the lattice neighbours, which is done by suitable destructive interference with a very weak Gaussian beam), we thread a helical beam through the origin which has twice the total intensity of each of the Gaussian lattice beams (Fig. 4 **B**). This construction demonstrates that a single dark helix can be embedded into a bright background.

Alternatively, the entire lattice is formed from helical beams with equal strength (Fig. 4 **C**). In both cases the intensity at the helix cores is suppressed by at least four orders of magnitude (Fig. 4 **B** and **C**).

Such intensity helices of light may turn out to be applied in nanolithography of bulk media [24] to create sharply contoured helical imprints in potentially massively parallel fashion. Their defined handedness might help, e.g., with the production of chiral meta-

materials [25].

Filtering of handed molecules, through a membrane with photo-lithographically etched helical holes or via handedness-sensitive trapping in solution, might become possible.

For the manipulation of ultra-cold gas clouds via the optical dipole force, dark (blue-detuned) and bright (red-detuned [8]) helical beams may turn out to be useful [23]. The helices can be made to intertwine, opening up the possibility of studying intertwined transport. In the presence of gravity or other uniform force fields a helix that is tilted away from vertical by more than its pitch angle can potentially serve as a microscopic Archimedean-screw transporter [11] or a helical ratchet-potential. Transport along helices is expected to show localization behaviour [26, 27] and other interesting quantum-transport phenomena [28].

1. L. Allen, M. W. Beijersbergen, R. J. C. Spreeuw, and J. P. Woerdman, Phys. Rev. A **45**, 8185 (1992).
2. M. Padgett and L. Allen, Cont. Phys. **41**, 275 (2000).
3. M. Padgett, J. Courtial, and L. Allen, Physics Today **57**, 35 (2004).
4. M. Harris, C. A. Hill, and J. M. Vaughan, Opt. Commun. **106**, 161 (1994).
5. J. M. Vaughan, Journal of Optics A: Pure and Applied Optics **1**, 750 (1999).
6. J. Leach, S. Keen, M. J. Padgett, C. Saunter, and G. D. Love, Optics Express **14**, 11919 (2006).
7. K. Staliunas (1999), arXiv:cond-mat/9912268.
8. M. Bhattacharya, Opt. Commun. **279**, 219 (2007), arXiv:0707.1916.
9. K. Volke-Sepúlveda and R. Jáuregui, J. Phys. B: At. Mol. Phys. **42**, 085303 (2009), arXiv:quant-ph/0812.0090.
10. J. F. Nye and M. V. Berry, Royal Society of London Proceedings Series A **336**, 165 (1974).
11. S. Kuhr, W. Alt, D. Schrader, M. Müller, V. Gomer, and D. Meschede, Science **293**, 278 (2001).
12. D. Meschede and H. Metcalf, J. Phys. D: Appl. Phys. **36**, R17 (2003).
13. O. Steuernagel, Am. J. Phys. **73**, 625 (2005), arXiv:physics/0312116v2.
14. L. Marrucci, C. Manzo, and D. Paparo, Phys. Rev. Lett. **96**, 163905 (2006).
15. J. Leach, M. R. Dennis, J. Courtial, and M. J. Padgett, Nature **432**, 165 (2004).
16. M. P. MacDonald, L. Paterson, K. Volke-Sepulveda, J. Arlt, W. Sibbett, and K. Dholakia, Science **296**, 1101 (2002).
17. F. Pampaloni and J. Enderlein (2004), arXiv:physics/0410021.
18. L. Paterson, M. P. MacDonald, J. Arlt, W. Sibbett, P. E. Bryant, and K. Dholakia, Science **292**, 912 (2001).
19. J. Lekner, J. Opt. A: Pure Appl. Opt. **6**, L29 (2004).
20. K. Dholakia, G. C. Spalding, and M. MacDonald, Phys.World **15**, 31 (2002).
21. M. P. MacDonald, K. Volke-Sepulveda, L. Paterson, J. Arlt, W. Sibbett, and K. Dholakia, Opt. Commun. **201**, 21 (2002).
22. S. W. Hell, Science **316**, 1153 (2007).
23. S. Chu, Rev. Mod. Phys. **70**, 685 (1998).
24. S. Kawata, H.-B. Sun, T. Tanaka, and K. Takada, Nature **412**, 697 (2001).
25. A. Sihvola, Metamaterials **1**, 2 (2007).
26. Y. B. Gaididei, P. L. Christiansen, P. G. Kevrekidis, H. Büttner, and A. R. Bishop, New Journal of Physics **7**, 52 (2005), arXiv:nlin/0409010.
27. P. Exner and M. Fraas, Phys. Lett. A **369**, 393 (2007), arXiv:quant-ph/0704.2770.
28. X.-L. Qi and S.-C. Zhang (2008), arXiv:cond-mat/0810.5114.